Heath Monitoring of Capacitors and Supercapacitors Using Neo Fuzzy Neural Approach

Abdenour Soualhi, Maawad Makdessi, Ronan German, Francklin Rivas, Hubert Razik, Ali Sari, Pascal Venet, Guy Clerc

Heath Monitoring of Capacitors and Supercapacitors Using Neo-Fuzzy Neural Approach

Abdenour Soualhi, Maawad Makdessi, Ronan German, Francklin Rivas, Hubert Razik, *Senior Member*, *IEEE*, Ali Sari, Pascal Venet, *Senior Member*, *IEEE*, Guy Clerc, *Senior Member*, *IEEE*.

***Abstract*—Despite their great improvements, reliability and availability of power electronic devices remain always a focus. In safety-critical equipment, where the occurrence of faults can generate catastrophic losses, health monitoring of most critical components is absolutely needed to avoid and prevent breakdowns. In this paper, a noninvasive health monitoring method is proposed. It is based on fuzzy logic and the neural network to estimate and predict the equivalent series resistance (ESR) and the capacitance (C) of capacitors and supercapacitors. This method, based on the neo-fuzzy neuron model, performs a real-time processing (time series prediction) of the measured device impedance and the degradation data provided by accelerated ageing tests.**

To prove the efficiency of the proposed method, two experiments were performed. The first one was dedicated to the estimation of the ESR and C for a set of 8 polymer film capacitors, while the second one was dedicated to the prediction of the ESR and C for a set of 18 supercapacitors. The obtained results showed that combining fuzzy logic and the neural network is an accurate approach for the health monitoring of capacitors and supercapacitors.

***Index Terms*—prognosis, ageing, capacitor, supercapacitor, artificial neural network, fuzzy logic, time series prediction, health monitoring, parameter estimation**

I. INTRODUCTION

Currently, most of transportation systems contain embedded electronics equipment providing various functions (conversion, energy storage, control, etc.) [1]-[4]. For an increased lifetime expectation and safety of these components, strong efforts have therefore been devoted to improve reliability of power electronic systems with cost-effective and sustainable solutions [5]-[7].

Condition monitoring and health management present fundamental ways to improve the lifetime expectation of power devices. In this paper, we focus our study on the health monitoring of energy storage systems (ESS), particularly on metallized polymer film (MPF) capacitors and supercapacitors (SCs). The reliability of these components is a major issue since chemical solvents (such as acetonitrile, which is classified as hazardous) used for SCs and acetylene (noxious gases) for MPF capacitors may be released in the case of breakdown. Thus, the degradation of (ESS) performance must be monitored in order to avoid power breakdown or system malfunctioning.

SCs [8] are intermediate components between batteries (used for their very high energy density) and capacitors (mostly used for high frequency filtering). These components, also called ultracapacitors or electrochemical double layer capacitors, use an electrostatic mode to store energy (double layer effect). SCs present higher cyclability and higher specific power than other ESS based on electrochemical transformation such as batteries [9]; which is why SCs are appreciated in applications requiring a short duration power boost, such as regeneration of braking energy or stop and start systems.

MPF capacitors, on the other hand, present higher power density but lower energy density than SCs. Such components offer great advantages compared to other capacitor technologies, since they have the ability to self-heal. Indeed, thanks to this feature, MPF capacitors tend to generally fail within an open-circuit failure mode (gradual loss of electrode surface) rather than in a short-circuit one. MPF capacitors are also known for their low dissipation factor and high dielectric stability with frequency and temperature, which are important factors for filtering, power factor correction, and high temperature applications.

Accelerated ageing tests conducted on both capacitors and SCs showed that most of their failure modes can be monitored by the evolution of their precursor parameters of equivalent series resistance (ESR) and capacitance (C) [10]-[14]. Thus, an effective and reliable monitoring method must be based on the double estimation and/or prediction of these electrical parameters.

Even though failure modes and failure mechanisms are well known for a component, their estimation/prediction remains difficult to obtain, especially when electrical and environmental stresses are combined together. These constraints require the use of suitable diagnostic or prognostic methods to analyze the C and ESR in order to improve the health monitoring of SCs and MPF capacitors.

The objective of this paper is to limit such drawbacks and to show that with the same model (MPF capacitors and SC in our case), it is possible to detect potential deterioration drifts of different energy storage devices

II. CHOICE OF A HEALTH MONITORING METHOD

Model-based (or physics-based) methods and data-driven methods are often used to monitor ESS degradation [15]-[17]. The model-based method uses an analytical model to estimate and predict electrical parameters of components, while the data-driven method does not require a physical modeling of the components and aims to model the relationship between the measured data and the component degradation. The choice of a method is based on the complexity of the studied component and also on the availability of information about the component. Research conducted by [18] allowed extracting a comparison between these methods. The obtained

results led to favor in our case the data-driven method; although this mainly depends on the application.

From literature, artificial intelligence is the most popular data-driven method used for health monitoring. More specifically, artificial neural networks (ANNs) appear as a reliable technology for diagnosis and prognosis. Two types of ANNs exist: the feed forward neural networks and the recurrent neural networks [19]. These two types of ANNs have been successfully used for diagnosis and prognosis. However, some authors highlight some drawbacks:

- ANNs are black boxes and it is not possible to explain and analyze the relationship between inputs and outputs;
- ANNs are prone to over fitting.

Thus, to overcome these weaknesses, researchers combined the ANNs with fuzzy logic to obtain the neuro-fuzzy system (NFS). The use of the NFS for diagnosis/prognosis purposes requires taking into account the time factor and therefore generates a great computational burden. In this context, we propose to improve the architecture of the NFS by a new architecture named the neo-fuzzy neuron model (NFN). To explain how the NFS architecture is improved, consider an adaptive neuro-fuzzy system (ANFIS) with four inputs denoted $\{x_0, x_1, x_2, x_3\}$ and one output denoted $\hat{x}$ (see Fig.1). If two fuzzy sets (defined by triangular, trapezoidal or Gaussian membership functions) are associated with each input, the system will contain 16 fuzzy rules (4^2) =16. These rules are given as follows:

$$\text{Rule}(k): \quad \text{If } \left(x_0 \text{ is } \mu_{j0}\right) \text{ and } \left(x_1 \text{ is } \mu_{j1}\right) \text{ and } \left(x_2 \text{ is } \mu_{j2}\right) \text{ and } \left(x_3 \text{ is } \mu_{j3}\right), \quad j = 1,2$$

$$\text{Then } \hat{x}^k = f_k(x_0, x_1, x_2, x_3) = c_0^k x_0 + c_1^k x_1 + c_2^k x_2 + c_3^k x_3 + c_4^k, \quad k = 1,2,...16$$

Where (k = 16) is the number of rules, x_i for (i = 0, 1, 2, 3) is the i^{th} input and $\hat{x}^k$ is the output of rule (k). μ_{ji} is the j^{th} membership function of the input x_i and $\{c_0^k, c_1^k, c_2^k, c_3^k, c_4^k\}$ are the coefficients of rule (k).

The structure of the ANFIS predictor contains five layers including the input layer (see Fig. 1). They are defined as follows:

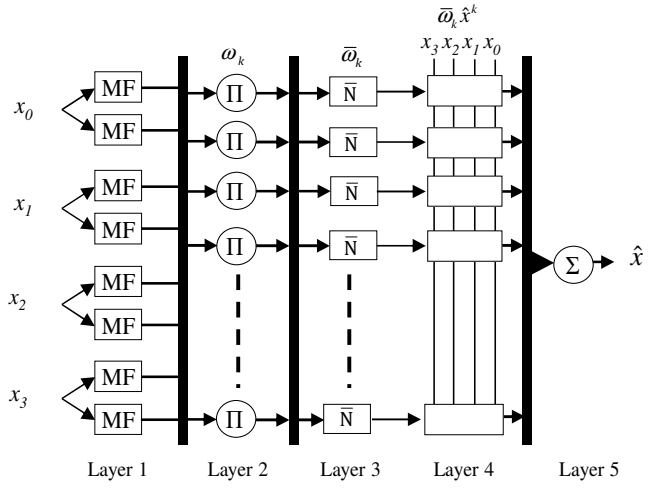

Fig.1. Architecture of adaptive neuro-fuzzy system for four inputs and two membership functions (MF).

Layer 1 membership function (MF): each input is associated with a MF which evaluates the membership degree of the j^{th} fuzzy partition with the i^{th} input variable. Here, the MF can be any function (triangle, trapezoid or Gaussian). For a Gaussian function, we have:

$$\mu_{ji}(x_i) = \exp\left(-\left[\frac{x_i - m_{ji}}{b_{ji}}\right]^2\right) \tag{1}$$

with (m_{ji}, b_{ji}), the Gaussian function parameters (premise parameters).

Layer 2 (Π): in this layer, the weight ω_k of each rule (k) is associated with the MF of each input by using a T-norm. The most widely used T-norm is the product:

$$\omega_k = \mu_{j0}(x_0) \cdot \mu_{j1}(x_1) \cdot \mu_{j2}(x_2) \cdot \mu_{j3}(x_3) \tag{2}$$

Layer 3 ($\bar{\text{N}}$) : the purpose of this layer is the normalization of the different weights. The normalization is expressed as follows:

$$\bar{\omega}_k = \omega_k \Big/ \sum_{k=1}^{16} \omega_k \tag{3}$$

Layer 4 : this layer computes the contribution of each rule (k) by a first-order input function (Takagi-Sugeno approach):

$$\bar{\omega}_k \hat{x}_{t+p}^k = \bar{\omega}_k \cdot \left(c_0^k x_0 + c_1^k x_1 + c_2^k x_2 + c_3^k x_3 + c_4^k\right) \tag{4}$$

with $\{c_0^k, c_1^k, c_2^k, c_3^k, c_4^k\}$ the coefficients of this linear combination and are called consequent parameters.

Layer 5 (Σ): the output of this layer is the sum of all incoming rules.

$$\hat{x} = \sum_{k=1}^{16} \bar{\omega}_k \hat{x}^k = \sum_{k=1}^{16} \bar{\omega}_k \cdot \left(c_0^k x_0 + c_1^k x_1 + c_2^k x_2 + c_3^k x_3 + c_4^k\right) \tag{5}$$

The goal of the ANFIS system is to form an adaptive network able to approximate an unknown function through the learning data and then find the precise values of the parameters above (consequent and premise parameters). The characteristic of this approach is that ANFIS applies a hybrid learning algorithm. The hybrid learning algorithm is an association between the gradient descent method and the least squares method. The gradient descent method is used to adjust the premise parameters (m_{ji}, b_{ji}), whereas the least squares method is used to identify the consequent parameters $\{c_0^k, c_1^k, c_2^k, c_3^k, c_4^k\}$. The inconvenient of the ANFIS system is related to a slow convergence of the learning step when the number of membership functions is big and/or when the number of inputs is big. To solve this problem, we propose the use of a new NFS called the NFN [20]. The architecture of a NFN is quite close to an artificial neural network architecture with several inputs. However, instead of the usual synaptic weights, it contains nonlinear synapses. Among the most important advantages of the NFN model are the high rate of learning, simplicity of calculation, and also that it is characterized by the fuzzy rules of "if-then".

The present paper is focused on the monitoring of MPF capacitors and SCs. More precisely, the objective of this paper is to show how it is possible to use the NFN model to estimate

the ESR in the case of the MPF capacitor and to predict the evolution of the ESR and C in the case of SCs.

III. Health Monitoring of SCs

A. SCs ageing indicators

From literature, SCs ageing leads to C decrease and ESR increase (see Fig.2). The decrease in C and the increase in ESR are not totally linked together as they are not related to the same phenomena (storage surface decrease for C and separator gas storage, internal pressure increase and contact degradation for ESR). Some publications define end of time parameters for SC life prediction [12], but we will focus on the study of C and ESR through time. So instead of having only one information (i.e., the lifetime), one can monitor and predict the evolution of SC parameter through time.

B. SCs ageing factors

As SC ageing time is quite long under nominal conditions, some accelerated ageing tests are performed [12], [21]. The goal of those tests is to shorten the ageing test duration without implying any new ageing mode. Basically, they need voltage to take place and temperature plays the role of an acceleration factor [22], as long as the temperature is within the operating range of the SC [12]. For out of bonds temperatures, new ageing mechanisms will happen but it is not the target of this paper.

Two kinds of accelerated ageing tests are usually performed. They are called cycling and floating ageing [22]. Cycling ageing consists of charging and discharging the SC in cycles. The loss of C and increase of ESR are very fast, but ageing is mainly reversible [23]. The acceleration factors for cycling ageing are depth of discharge, temperature and the root mean square (RMS) value of the current [12]. Floating ageing consists of maintaining the voltage and temperature of SC as constant as possible through time. Thus, only temperature and voltage are ageing factors, since RMS current is near to 0 A. This kind of ageing is mainly irreversible.

Our study will focus on floating ageing since it is the main ageing mode for personal vehicles (95% of the time) and uninterruptible power supplies (99% of the time) and because it is an irreversible ageing mode. Thus, we will not study variable ageing constraints.

Fig. 2 presents averaged ageing results for floating ageing tests for 3 groups of three SCs aged with different constant voltage and temperature constraints. The results are presented in percent compared to the manufacturer rated C and ESR. The effect of temperature and voltage can be easily deduced. The reference test (60°C, 2.8 V) showed that a lower temperature (50°C, 2.8 V) or a lower voltage (60°C, 2.3 V) led to lower ageing speed.

As most of the SC used in hybrid and electric vehicles are based on the acetonitrile/activated carbon technology, the increase of ESR and the decrease of C through time have the same shape. Thus, although the parameter values from the learning database will not be the same for another SC, the method developed in this paper is applicable to other acetonitrile/ activated carbon SCs.

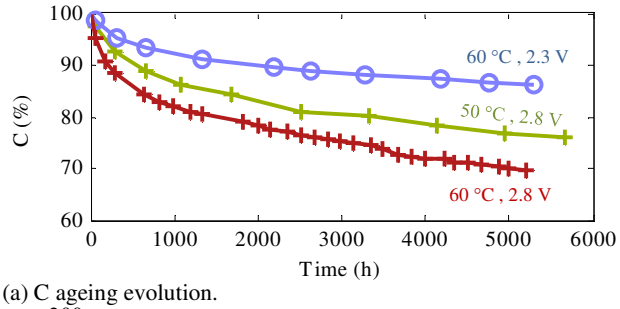

(a) C ageing evolution.

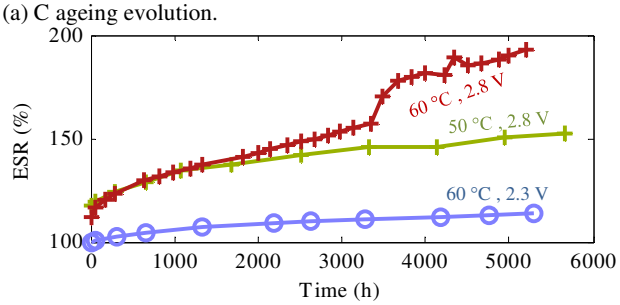

(b) ESR ageing evolution.

Fig. 2. Impact of ageing on supercapacitor capacitance (C) and equivalent series resistance (ESR) for different accelerated calendar ageing test.

C. Prediction of the ESR and C for SCs

The C and resistance of the tested SC were measured at 100 mHz by electrochemical impedance spectroscopy (EIS) [23]. For any high power/ high C of SC, the impedance behavior is similar to the impedance of distributed porous electrodes [24]. The C of SC is frequency dependent and goes to its maximum value at low frequency [22]. Testing the SC at 100 mHz was a good compromise between capacitance estimation and acquisition time. Thus we used that frequency for C and ESR calculation.

$$C = \left. \frac{1}{-j.\mathrm{Im}(Z_{SC})\omega} \right|_{@100mHz} \tag{6}$$

$$ESR = \mathrm{Re}(Z_{SC})\big|_{@100mHz} \tag{7}$$

with $\mathrm{Im}(Z_{SC})$ and $\mathrm{Re}(Z_{SC})$ the imaginary and real parts of the SC impedance (Z_{SC}) measured at 100 mHz.

This kind of estimation for C and ESR has the advantage of taking only experimental data without any other data treatment. With the selected SCs and the measurement tools used for the paper, the reproducibility of the extracted C and ESR were inferior to 0.5%. Other publications use data fitting for the identification of the SC model [25], [22]. The fitting is used to analyze experimental curves. It consists on constructing a curve from mathematical functions and adjusting the parameters of these functions to approximate the measured curve. For simple cases, the linear regression is used if the curve is linear for all parameters, or polynomial regression when using a polynomial to simulate the phenomenon (the degradation of SCs in our case). Conventional regression methods make possible to determine the mathematical functions from the data of the curve but are inapplicable if the function takes into account physical parameters not available in the curve, such as the temperature and the supply voltage, which are necessary to provide a good estimation of ESR and C.

As mentioned previously, the ageing of SCs can be predicted by estimating the evolution of ESR and C. This estimation is based on the following assumption.

Consider a set of measures denoted "X" performed on a SC. These measures are used to estimate an unobservable measure denoted $\hat{x}_{t+p}$ via the function $f(X)$. This function is expressed as follows:

$$\hat{x}_{t+p} = f(X) = f(V_t, \theta_t, x_{t-(n-2)r} \ldots x_{t-3r}, x_{t-2r}, x_{t-r}, x_t) \quad (8)$$

$\hat{x}_{t+p}$ is a measure "x" estimated for a horizon of prediction denoted p. The measure "x" corresponds to the ESR if the unobservable measure is $E\hat{S}R_{t+p}$ and corresponds to the C if the unobservable measure is $\hat{C}_{t+p}$. x_t is a measure acquired at time t. x_{t-r} is a measure acquired at time t-r, where r is the interval between two measures (expressed in hours). $x_{t-(n-2)r}$ is a measure acquired at time t-$(n$-$2)r$, where n represents the number of measures. V_t, θ_t are respectively the supply voltage V_t and the temperature θ_t. The ageing estimation of the SC is illustrated in Fig. 3 for $\hat{C}_{t+p}$ with r=100, n=7 and p=2600, 3000 h...

Figure 4 represents the architecture of the proposed NFN model. The output of the NFN is expressed as follows:

$$\hat{x}_{t+p} = f(X) = \sum_{i=0}^{n} f_i(\bar{x}_i) \quad (9)$$

Where $f(X)$ results by the sum of nonlinear functions $f_i(\bar{x}_i)$. Each function f_i is related to a normalized input $\bar{x}_i$ which represents the i^{th} position of the series "X". The last and before the last position of the series "X" represent respectively the supply voltage and the temperature of the SC, $\bar{x}_n = \bar{V}_t$, $\bar{x}_{(n-1)} = \bar{\theta}_t$. The normalized input $\bar{x}_i$ is comprised between 0 and 1 ($0 \leq \bar{x}_i \leq 1$) and is defined by the following formula:

$$\bar{x}_i = \frac{x_i}{x_{max}} \quad (10)$$

where x_{max} is the maximal value recorded in the training step.

The function $f_i(\bar{x}_i)$ depends on the interconnecting weights ω_{ji} between the i^{th} input $\bar{x}_i$ and the j^{th} membership value $\mu_{ji}(\bar{x}_i)$. The function $f_i(\bar{x}_i)$ is expressed as follows:

$$f_i(\bar{x}_i) = \sum_{j=1}^{h} \omega_{ji} \cdot \mu_{ji}(\bar{x}_i) \quad (11)$$

Where h is the number of MF.

The membership values are obtained from triangular functions spaced equivalently according the number (h) of MFs as shown in Fig. 5.

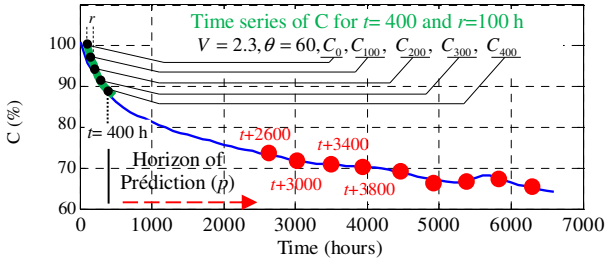

Fig. 3. Prediction of the capacitance until a horizon p from X_C.

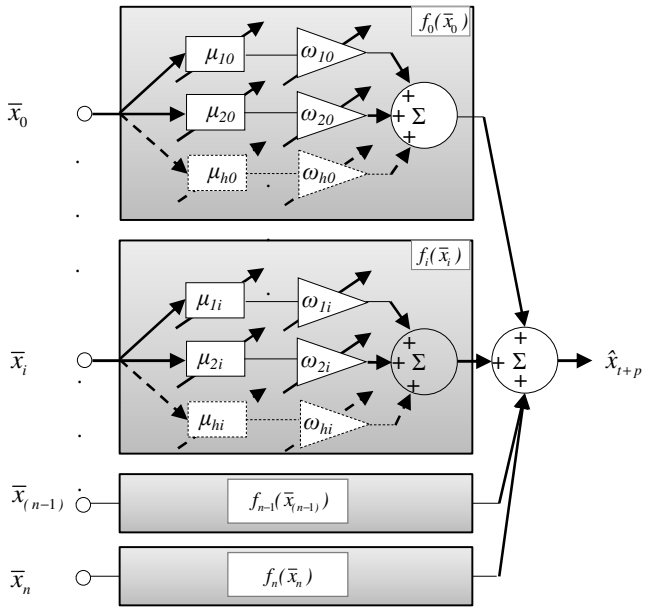

Fig. 4. Architecture of a neuro-fuzzy neuron model for the prediction of equivalent series resistance and capacitance.

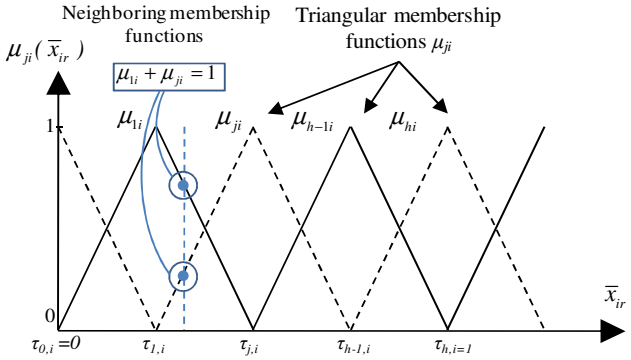

Fig. 5. General view of triangular membership functions.

$\tau_{0,i}$, $\tau_{1,i}$,..., $\tau_{j,i}$,, $\tau_{h,i}$ are the positions of the triangular functions with $\tau_{h,i}$= 1. They are comprised between 0 and 1 ($0 \leq \tau_{j,i} \leq 1$). They are defined according to the number of the MF h. For h MFs, the position $\tau_{j,i}$ is equal to j/h.

The membership value $\mu_{ji}(\bar{x}_i)$ is obtained according to the i^{th} input in the intervals $[\tau_{j-1,i}, \tau_{ji}]$ and $[\tau_{ji}, \tau_{j+1,i}]$. $\mu_{ji}(\bar{x}_i)$ is expressed as follows:

$$\mu_{ji}(\bar{x}_i) = \begin{cases} \dfrac{\bar{x}_i - \tau_{j-1,i}}{\tau_{ji} - \tau_{j-1,i}} & , \bar{x}_i \in [\tau_{j-1,i}, \tau_{ji}] \\ \dfrac{\tau_{j+1,i} - \bar{x}_i}{\tau_{j+1,i} - \tau_{ji}} & , \bar{x}_i \in [\tau_{ji}, \tau_{j+1,i}] \\ 0 & \text{otherwise} \end{cases} \quad (12)$$

Based on equation (11) and Fig. 5, the output value of the nonlinear synapse $f_i(\bar{x}_i)$ depends only on two neighboring MFs (j, j+1). $f_i(\bar{x}_i)$ is expressed as follows:

$$f_i(\bar{x}_i) = \omega_{ji} \cdot \mu_{ji}(\bar{x}_i) + \omega_{j+1,i} \cdot \mu_{j+1,i}(\bar{x}_i) \quad (13)$$

Finally, the estimation of $\hat{x}_{t+p}$ is given by:

$$\hat{x}_{t+p} = f_0(\bar{x}_0) + f_i(\bar{x}_i) + \ldots + f_n(\bar{x}_n) \quad (14)$$

where t denotes current time instant, $\hat{x}_{t+p}$ is the estimated value at the horizon $t+p$.

The interconnecting weights are calculated in the training step after ℓ-iterations by considering equation (9), where the output of the NFN model is expressed as follows:

$$\hat{x}_{t+p}(\ell) = \sum_{i=0}^{n} f_i(\bar{x}_i(\ell)) = \sum_{i=0}^{n}\sum_{j=1}^{h} \omega_{ji}(\ell-1)\mu_{ji}(\bar{x}_i(\ell)) \quad (15)$$

The output $\hat{x}_{t+p}(\ell)$ depends on the MFs $\mu_{ji}(\bar{x}_i)$ and the adjustable weights $\omega_{ji}(\ell\text{-}1)$ obtained from the previous iteration. Therefore, there are $n \times h$ weights to be adjusted according to a criterion. This criterion consists on updating the synaptic weights by minimizing the quadratic error function E(ℓ) which is expressed as follows:

$$\begin{aligned} E(\ell) &= \frac{1}{2}(x_{t+p}(\ell) - \hat{x}_{t+p}(\ell))^2 = \frac{1}{2}e(\ell)^2 \\ &= \frac{1}{2}(x_{t+p}(\ell) - \sum_{i=0}^{n}\sum_{j=1}^{h} \omega_{ji}(\ell-1)\mu_{ji}(\bar{x}_i(\ell)))^2 \end{aligned} \quad (16)$$

The quadratic error is minimized by the gradient descent algorithm which allows calculating ω_{ji} by the following formula:

$$\begin{aligned} \omega_{ji}(\ell+1) &= \omega_{ji}(\ell) + \rho\, e(\ell+1)\mu_{ji}(\bar{x}_i(\ell+1)) \\ e(\ell+1) &= x_{t+p}(\ell+1) - \sum_{i=0}^{n}\sum_{j=1}^{h} \omega_{ji}(\ell)\mu_{ji}(\bar{x}_i(\ell+1)) \end{aligned} \quad (17)$$

This equation depends on three parameters. The first parameter is the learning rate ρ, comprised between 0 and 1, used to control the convergence of the learning process. The second parameter is the MF μ_{ji} calculated in equation (12). The third is the real measure x_{t+p}.

IV. Health Monitoring of MPF Capacitors

A. MPF ageing

MPF ageing leads to a variation in C and ESR. Table I resumes the ESR and C evolutions depending on the applied stresses [26]. Based on the different failure mechanisms shown in Table I, it seems extremely important to monitor both the ESR and C, since all of the failures mechanisms can be detected through the evolution of these electrical parameters.

TABLE I
Comparison Between Capacitance (C) and Equivalent Series Resistance (ESR) Evolutions Under Different Stresses

Ageing tests	Standard ageing at constant voltages and temperatures	High ripple currents	High ripple current with a dc voltage	High current pulses
Drawbacks	ESR ↗↗	ESR ↗	ESR ↗↗	ESR ↗↗
	C ↘	C ↘↘	C ↘↘	C →

B. MPF ageing factors

Different factors may have an irreversible impact on performance of MPF capacitors with time and deteriorate their operating lifetime. Among the numerous ageing factors, voltage and temperature are the most prevalent stresses [28].

Two kind of accelerated ageing test are usually performed. (i) Standard ageing by "floating", at a fixed temperature and voltage. This makes possible to analyze the behavior of the capacitor parameters as a function of time and therefore determining the acceleration factors of voltage and temperature. (ii) Ageing by current ripple with the application of a zero DC voltage. This type of ageing generates degradation of the metallization by electrochemical corrosion with superposition of a DC voltage to the above mentioned current ripple [27], [28]. This test combines the constraints of the tests mentioned above (tests with the application of a current ripple and "floating") and consists of applying to the capacitor similar stresses encountered in a power electronics application. It makes it possible to study the impact of using the capacitor as a filter element of a static energy converter. In the following, standard ageing by "floating" is used to accelerate the ageing of MPF capacitors.

C. Estimation of the ESR and C for MPF capacitor

The health monitoring of an MPF capacitor consists of estimating the ESR and C. This estimation is obtained from the capacitor impedance, extracted within the frequency domain analysis. Indeed, if we plot Bode diagrams of a MPF 15µF-400 V capacitor at different ageing states, we note, as shown in Fig. 6, two distinct frequency regions separately dominated by ESR and C.

From the plotted curves, one can notice an evolution of the ESR and C for different ageing states. From theses curves, one can observe that the decrease of the capacitor impedance at low frequencies is followed by a decrease of the capacitance impedance at the resonant frequency (f_{res}). This is interpreted by a link between the C and ESR. The C is estimated using (18) at low frequencies where $1/(2\pi fC) >> ESR$:

$$C = \frac{1}{|Z_{MPF}| \cdot 2\pi f} \quad (18)$$

The ESR, estimated on the basis of its relation with C, is given by the NFN model where the output of the model is the ESR estimated at a time t denoted $\hat{ESR}_t$ and the inputs are a series of impedances noted Z_{fi} measured at different frequencies. This estimation is obtained by considering the following assumption.

Consider a series of impedances "Z" measured from an MPF capacitor. These measurements are used to estimate an unobservable parameter noted $\hat{ESR}_t$ via a function $f(Z)$. This function is expressed as follows:

$$\hat{ESR}_t = f(Z) = f(Z_{fn}, \ldots, Z_{f_2}, Z_{f_1}) \quad (19)$$

where n represents the number of impedance measures used for the estimation of the $\hat{ESR}_t$. In the case of the MPF capacitor, $n = 4$ corresponds to the impedances Z_{f1}, Z_{f2}, Z_{f3} and Z_{f4} measured respectively at 200, 300, 400 and 500 Hz at time t. The choice of the frequencies 200, 300, 400 and 500 Hz is justified by the fact that the impedance of the capacitor for frequencies higher than 500 Hz will be disturbed because of the low amplitudes of harmonics (i.e., Fig. 13). The $\hat{ESR}_t$ is the NFN output which corresponds to the ESR at the resonant frequency (~1 MHz).

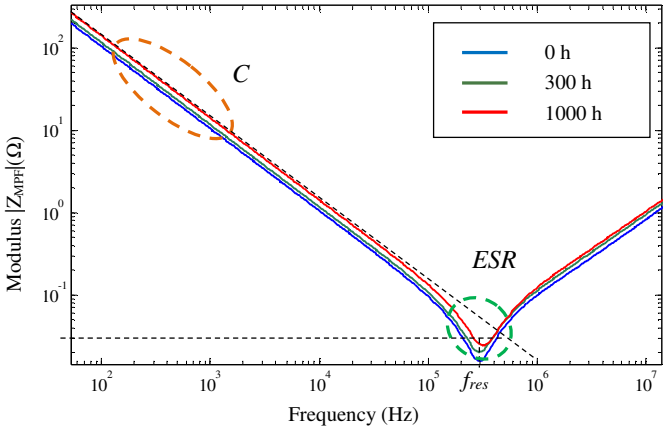

Fig. 6. Impact of ageing on capacitance (C) and equivalent series resistance (ESR) of a metallized polymer film capacitor for different accelerated ageing tests.

Since ESR values may differ from one capacitor to another (due to contact resistance), an additional input was introduced to the NFN model, that is $Z_{f0} = ESR_0$ corresponding to the ESR of the monitored component at its healthy state (t=0). Very often, most of the diagnostic techniques require the knowledge of the component initial state regardless of the exploited physical quantity.

Fig. 7 illustrates the inputs and output of the NFN model. The output of the NFN is expressed as follows:

$$E\hat{S}R_t = \sum_{i=0}^{n} f_i(\bar{Z}_{f_i}) \tag{20}$$

with $\bar{Z}_{f_i}$ a normalized impedance (observation) situated in the i^{th} position of the impedance series. The first position of the impedance series represents the normalized ESR at the healthy state $\bar{Z}_{f_0} = \overline{ESR}_0$.

The function $f_i(\bar{Z}_{f_i})$ is formulated as follows:

$$f_i(\bar{Z}_{fi}) = \sum_{j=1}^{h} \omega_{ji} \cdot \mu_{ji}(\bar{Z}_{fi}) \tag{21}$$

Where ω_{ji} are the interconnecting weights between the i^{th} input $\bar{Z}_{fi}$ and the j^{th} membership value $\mu_{ji}(\bar{Z}_{fi})$.

As for SCs, the membership values $\mu_{ji}(\bar{Z}_{fi})$ are extracted from triangular functions spaced equivalently according the number (h). $\mu_{ji}(\bar{Z}_{fi})$ is expressed as follows:

$$\mu_{ji}(\bar{Z}_{fi}) = \begin{cases} \dfrac{\bar{Z}_{fi} - \tau_{j-1,i}}{\tau_{ji} - \tau_{j-1,i}} & , \bar{Z}_{fi} \in \left[\tau_{j-1,i}, \tau_{ji}\right] \\ \dfrac{\tau_{j+1,i} - \bar{Z}_{fi}}{\tau_{j+1,i} - \tau_{ji}} & , \bar{Z}_{fi} \in \left[\tau_{ji}, \tau_{j+1,i}\right] \\ 0 & \text{otherwise} \end{cases} \tag{22}$$

The function $f_i(\bar{Z}_{f_i})$ depends only on two neighboring membership functions (j, j+1). It is expressed as follows:

$$f_i(\bar{Z}_{fi}) = \omega_{ji} \cdot \mu_{ji}(\bar{Z}_{fi}) + \omega_{j+1,i} \cdot \mu_{j+1,i}(\bar{Z}_{fi}) \tag{23}$$

The weight ω_{ji} is updated by a learning process based on the same principle of (17).

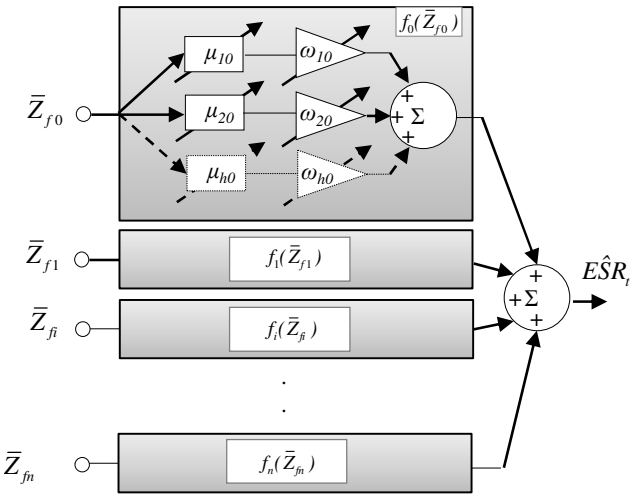

Fig. 7. Neo-fuzzy neuron (NFN) architecture for the equivalent series resistance (ESR) estimation.

Finally, The estimation of $E\hat{S}R_t$ is given by:

$$E\hat{S}R = f_0(\bar{Z}_{f0}) + \ldots + f_i(\bar{Z}_{fi}) + \ldots + f_n(\bar{Z}_{fn}) \tag{24}$$

V. Experimental Setup

A. Health monitoring of SCs

1) SC test bench for ESR and C prediction

Fig. 8 shows the test bench used to obtain the experimental ageing results for ESR and C evolution. Nine independent DC voltage sources were used to maintain a fixed voltage constraint for 9 SCs. A first group of 3 SCs was aged at 2.8 V, 3 other SCs were aged at 2.7 V and the last 3 SCs group was aged at 2.3 V. A programmable thermal chamber allowed fixing a temperature constraint equal to 60°C for all SCs. Then a second batch of 9 SCs was aged at 50 °C within the same voltage constraints. Thus, a total amount of 18 SCs were tested. Those ageing results were used for building the learning and test database. A 4-point connection was realized due to the impedance of the SC which was in the same order of magnitude as the electrical wires (0.1 mΩ). An impedance spectrometer was used for the characterization of SCs. Some of the experimental results are presented in Fig. 2.

SCs are characterized by galvanostatic mode EIS (sinewave current imposed and voltage amplitude and phase measured) at ageing voltage (2.3 V, 2.7 V or 2.8 V).

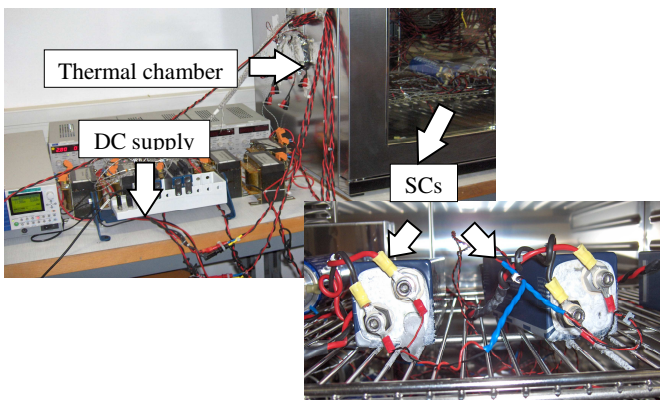

Fig. 8. Test bench for supercapacitor ageing.

The characterization frequency went from high frequency

(10 kHz) to the low frequency (10 mHz). The capacitor and the resistance were characterized at low frequency (100 mHz), see eq. (6) and (7), as the SC is used for low frequency applications (1 to 10 s power supply, braking energy recovery in electric vehicles, etc.).

2) Prediction of the ESR and C evolution

The prediction of the ESR and C passed by three steps: database creation, learning and validation.

- Step 1. *Database creation:* The learning database was created from 12 identical SCs of 3000 F and 2.7 V placed in a thermal chamber regulated at 60°C for the first batch of 6 SCs and 50°C for the second batch of 6 SCs. Each batch was divided into two groups, in which each one was supplied with a specific voltage (2.8 V for group 1 and 2.3 V for group 2). The ageing evolution of these components showed that SCs of the same group followed the same ageing evolution. These results validated our measuring method and therefore validated the learning database. This was obtained by characterizing each SC thanks to an impedance spectrometer.

- Step 2. *Learning*: To show the learning capability of the NFN model, consider a database composed of two SCs noted SC_1 and SC_3 supplied respectively with 2.8 V and 2.3 V at 60°C. Based on the learning database created in step 1, two NFN models were created based on the ageing of the 12 SCs supplied at 2.3 V and 2.8 V and placed at 50°C and 60°C. The first model was used to estimate the ageing of the ESR and the second model to estimate the ageing of the C. The input of the first NFN model included the time series X_{ESR} for SC_1 and SC_3. The interval between each measure was expressed in hours. This time series is defined as follows:

$$X_{ESR} = \{V_t, \theta_t, ESR_{t-400}, ESR_{t-300}, ESR_{t-200}, ESR_{t-100}, ESR_t\}$$

The second model included the time series X_C for SC_1 and SC_3. These time series are defined as follows:

$$X_C = \{V_t, \theta_t, C_{t-400}, C_{t-300}, C_{t-200}, C_{t-100}, C_t\}$$

The interval r between each measure was fixed to 100 h (r=100), (n-2) = 4, θ_t=60°C,V_t=2.3V for SC_3 and V_t=2.8V for SC_1. The output of the two models corresponded respectively to the estimation of the ESR and C, for a horizon of prediction (p) equal to 2600 h.

Two hundred triangular MFs (h=200) were used for each input of the NFN model. The interconnecting weights were updated in order to match the estimations values (prediction) with the desired ones.

The learning rate ρ was fixed according to normalized root mean square error (NRMSE). The NRMSE is the error between the estimation and the measure of the ESR and C. It is formulated as follows:

$$NRMSE = \frac{\sqrt{\frac{1}{N}\sum_{i=1}^{N}(y_i - \hat{y}_i)^2}}{y_{max} - y_{min}} \qquad (25)$$

where N represents the number of predicted values, y_i and $\hat{y}_i$ represent respectively the estimated and the real values of the i^{th} prediction. y_{max} and y_{min} are respectively the maximum and minimum values of the curve.

Figures 9(a) and 9(b) show the estimation results given by the two NFN models based on the learning database. The second step showed good results for a learning rate ρ = 0.5 with a NRMSE equal to 0.772*10^{-6} for the C and a NRMSE close to 0 for the ESR.

- Step 3. *Validation*: Figures 10(a) and (b) show respectively the ageing evolution of the ESR and C of a SC noted SC_2 supplied with 2.7 V at 60°C (blue curve). The input of the NFN was the time series X_{ESR} and X_C. The temperature θ_t=60°C and the voltage V_t was fixed to 2.7 V. Each input of the model was connected to 200 MF (h=200). The output of the model was the $\hat{ESR}_{t+p}$ and $\hat{C}_{t+p}$ with p = 2600 h (red curve). The NRMSE of the ESR and C were respectively 0.025 and 0.004. Table II gives the NRMSE of the ESR and C for different horizons of prediction (p= 100h, 1100h,...).

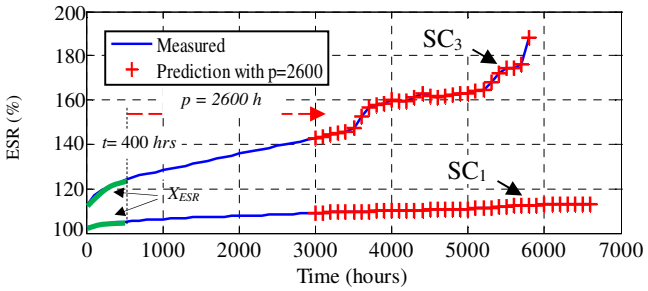

Fig. 9 (a). Learning result of the equivalent series resistance (ESR) neo-fuzzy neuron model for SC_1 (2.3 V, 60°C) and SC_3 (2.8 V, 60°C) with a horizon p=2600 h.

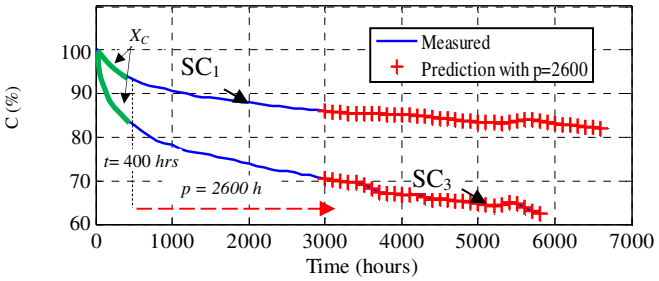

Fig. 9(b). Learning result of the capacitance (C) neo-fuzzy model for SC_1 (2.3 V, 60°C) and SC_3 (2.8 V, 60°C) with a horizon p=2600 h.

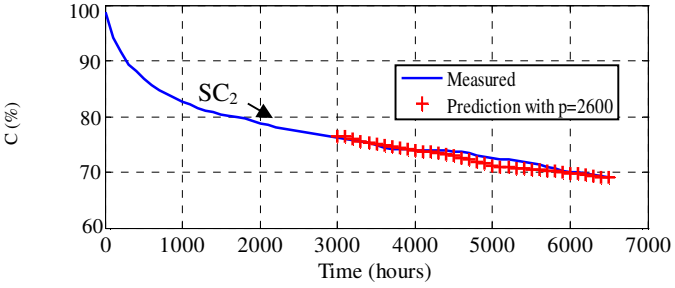

Fig. 10(a). Prediction of the capacitance (C) evolution for an accelerated ageing test of SC_2 (2.7 V, 60°C).

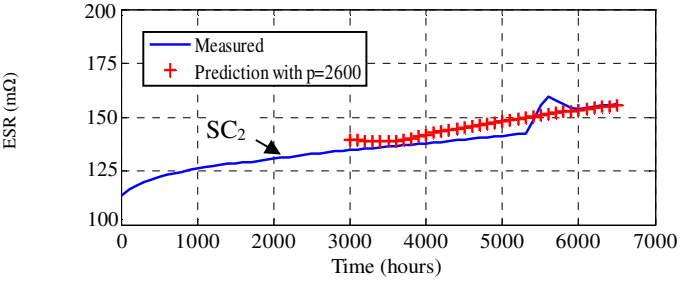

Fig. 10(b). Prediction of the equivalent series resistance (ESR) evolution for an accelerated ageing test of SC_2 (2.7 V, 60°C).

TABLE II
NORMALIZED ROOT MEAN SQUARE ERROR (NRMSE) OF THE EQUIVALENT SERIES RESISTANCE (ESR) AND CAPACITANCE C FOR SC_2

Horizon of prediction p (hours)	NRMSE (%)	
	ESR	C
100	**0.126**	**0.036**
1100	**0.249**	**0.041**
16000	**0.253**	**0.041**
26000	**0.290**	**0.043**
46000	**0.813**	**0.049**

Results of Table II show that the values of the NRMSE for the ESR and C are very small and therefore demonstrated that the introduction of the voltage and temperature in the time series of the ESR and C is a good strategy to predict the ageing of SCs. The peak in the ESR located after 5500 h (see Fig. 10(b)) was due to a stop of two weeks in the ageing process. The effect of ageing perturbation disappeared after a few times of relaunching. After that, the ESR increased normally.

The decrease in the C value indicated the degree of degradation in the contact surface between the electrolyte and the electrode of the SC. This decrease was interpreted by a decrease in energy storage capability.

The ageing of the ESR depends on the quality of contacts which are linked to the internal pressure of the SC. The increase in pressure causes a deformation of the SC, which can induce a breakdown in contacts. This defect is observable in Fig. 10 (a) where the value of the ESR jumps after 3500 h. This defect was not observable in the evolution of the C. This is why it is necessary to monitor simultaneously the evolution of the ESR and C.

B. Health monitoring of capacitors

1) MPF test bench

The test bench used for the ESR estimation was a switched mode power supply 230V AC/24V DC, 0-i_{Smax} as described in the block diagram of Fig. 11.

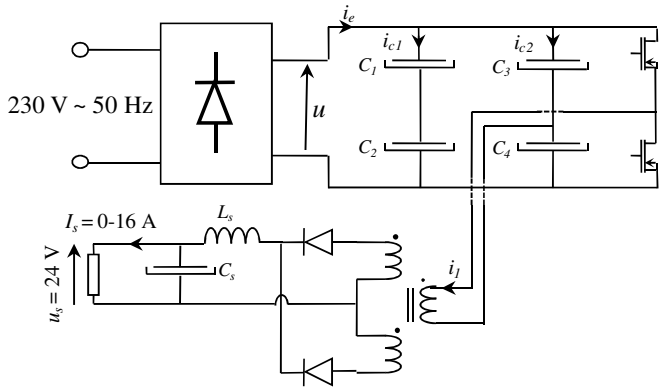

Fig. 11. Representation of the switched mode power supply.

Each of the input capacitors C_1, C_2, C_3 and C_4 was made of two MPF capacitors 15µF-400V connected in parallel.

2) Estimation of the ESR

- Step 1. *Database creation:*

The database was created from 8 identical MPF capacitors of 15µF-400V. These capacitors were subjected to a temperature constraint varying between 85°C and 100°C and a voltage constraint varying between 1.1 and 1.3·U_R. U_R is the capacitor rated voltage. The database was obtained by evaluating the impedance from the fast Fourier transform (FFT) of the current and voltage signals. The C was then calculated by using (18) at the low frequency and the ESR was estimated by the NFN model.

- Step 2. *Learning*:

This step considered the database of the MPF capacitor #1 (15µF-400V) supplied with 1.1·U_R at 85°C. This database was composed of an impedance series corresponding respectively to the frequencies (*fres*, 200 Hz, 300 Hz, 400 Hz and 500 Hz) and acquired at different time intervals (hours) during the ageing process. This database is summarized in Table III.

To test the accuracy estimation of the ESR by the NFN model, three MPF capacitors of 15µF-400V subjected to different electrical and thermal stresses were tested. The constraints are defined in Table IV.

ESR estimation results are given in Table V.

TABLE III
LEARNED DATABASE

Input / Time	Z_{fi} (mΩ)				
	frequency	200 Hz	300 Hz	400 Hz	500 Hz
0 *h*	**0.015**	**52.1**	**34.7**	**25.8**	**20.6**
150 *h*	**0.018**	**54.5**	**36.3**	**27**	**21.6**
350 *h*	**0.021**	**59.3**	**39.4**	**29.3**	**23.5**
850 *h*	**0.022**	**64.3**	**42.8**	**31.8**	**31.8**
1350 *h*	**0.023**	**70.2**	**46.7**	**34.7**	**27.8**

TABLE IV
TESTED CAPACITORS

MPF 15 µF	*# 2*	*# 4*	*# 6*
Temperature	**85°C**	**100°C**	**85°C**
Voltage	**1.1·U_R**	**1.1·U_R**	**1.3·U_R**

TABLE V
ESTIMATED EQUIVALENT SERIES RESISTANCE (ESR)

MPF 15 µF # 2					
Ageing time (h)	**50**	**150**	**350**	**850**	**1300**
ESR estimation error (%)	**2.5**	**2.2**	**5.8**	**0.9**	**3.8**
MPF 15 µF #4					
Ageing time (h)	**3**	**25**	**74**	**256**	**413**
ESR estimation error (%)	**2.5**	**0.18**	**3.4**	**1.5**	**1.8**
MPF 15 µF # 6					
Ageing time (h)	**5**	**26**	**43**	**85**	**116**
ESR estimation error (%)	**2.3**	**1.8**	**5**	**0.6**	**1.4**

The obtained results show that estimation errors of the ESR were small (error<5.8%). In addition, these results show that the introduction of ESR_0 in the impedance series allowed estimating the ESR of MPF capacitors subjected to electrical and thermal stresses which differed from those used in the learning phase.

- Step 3. *Validation*: *Online health monitoring*

Health monitoring was validated by measuring online the current and voltage across the capacitor C_3 where one of its MPF capacitor has been replaced by an aged component. The ageing process was simulated by replacing at specified

intervals (1300 h, 413 h, 113 h) the component forming C_3 by the MPFs (#2, #4, #6).

Figure 12 shows the curve of the current and voltage measured across the aged capacitor.

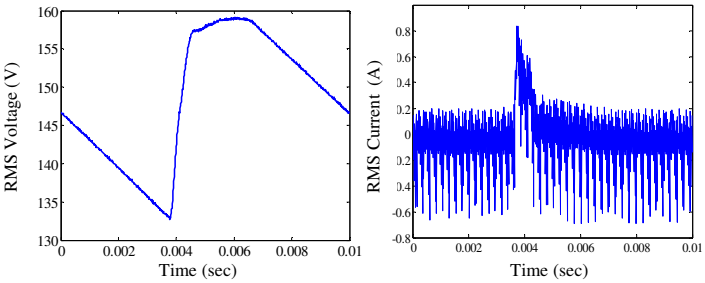

Fig. 12. Voltage and current signals corresponding to an aged capacitor.

After performing a FFT on the current and voltage signals, the impedance series Z_{fi} located at the frequencies (f_{res}, 200 Hz, 300 Hz, 400 Hz and 500 Hz) was extracted. The ESR_0, located in the resonance frequency was deduced before the ageing process thanks to an impedance spectrometer. Figure 13 shows the curve of the impedance Z_{MPF}. The blue curve represents the impedance identified online from the current and voltage signals. The red curve represents the impedance of the MPF capacitor measured from the impedance spectrometer. One can observe that the two curves are identical in the low band frequencies. This is why the impedance series is limited from 200 to 500 Hz. The estimated ESR and C given in Table VI show that the estimated values of ESR and C are coherent with those measured with an impedance meter, which proves the effectiveness of our approach.

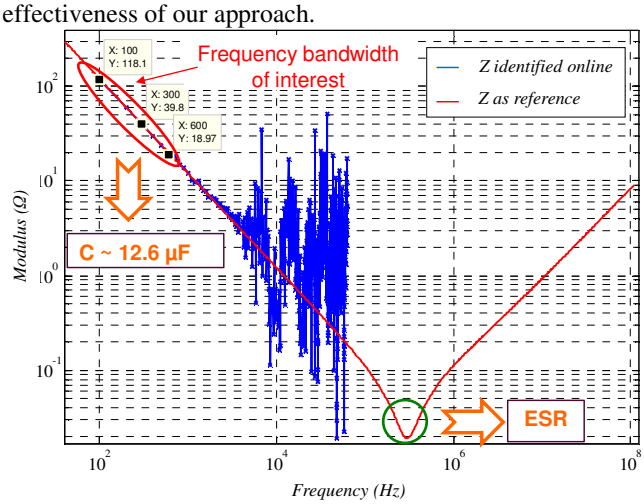

Fig. 13. Comparison between the impedance obtained from the voltage and current signals (blue curve) and the impedance measured by an impedance meter (red curve).

TABLE VI
ESTIMATED EQUIVALENT SERIES RESISTANCE (ESR) AND CAPACITANCE (C)

	MPF 15µF#2 at 1300 h	*MPF 15µF#4 at 413 h*	*MPF 15µF#6 at 116 h*
Electrical parameter	Estimated error (%)	Estimated error (%)	Estimated error (%)
C (µF)	**0.47**	**1.6**	**1.8**
ESR (mΩ)	**2.45**	**2.1**	**4.4**

VI. CONCLUSION

A model for the health monitoring of MPF capacitors and SCs based on the NFN model has been proposed in this paper. The bibliographical research showed that monitoring ESR and C is the best way for tracking the ageing of these components. For SCs, a time series composed by the ESR or C has been used in the NFN model. The obtained results showed that the introduction of temperature and voltage in this time series allow obtaining good predictions of ESR and C and therefore an accurate estimation of the remaining useful life. The same model was proposed for the estimation of ESR in the case of MPF capacitors. A series of impedances located in the low frequencies were used in the NFN model. Since ESR values may differ from one capacitor to another, an additional input was added to the impedance series, that is the ESR_0 corresponding to the healthy state. This strategy allows a robust and accurate estimation of the ESR. The proposed approach requires a database creation step and a learning step on a healthy and aged state. Further research is currently underway to implement the NFN predictor in complex industrial facilities and to develop new strategies for health monitoring and to generalize it to all ESS devices (batteries).

VII. REFERENCES

[1] H. Yhua, G. Chun, C. Wenping, L. Chushan, S.J. Finney, "Split Converter-Fed SRM Drive for Flexible Charging in EV/HEV Applications," *IEEE Trans. Ind. Electron.,* vol.62, no.10, pp.6085-6095, Oct. 2015.

[2] S.M. Lukic, J.Cao, R.C. Bansal, F. Rodriguez, A. Emadi, "Energy Storage Systems for Automotive Applications," *IEEE Trans. Ind. Electron.,* vol.55, no.6, pp.2258-2267, June. 2008.

[3] S.S. Williamson, A.K. Rathore, F. Musavi, "Industrial Electronics for Electric Transportation: Current State-of-the-Art and Future Challenges," *IEEE Trans. Ind. Electron.,* vol.62, no.5, pp.3021-3032, May. 2015.

[4] R. Bojoi, A. Cavagnino, A. Tenconi, S.Vaschetto, "Control of Shaft-Line-Embedded Multiphase Starter/Generator for Aero-Engine," *IEEE Trans. Ind. Electron.,* vol.63, no.1, pp.641-652, Jan. 2016.

[5] H. Shibuya and K. Kondo, "Designing Methods of Capacitance and Control System for a Diesel Engine and EDLC Hybrid Powered Railway Traction System," *IEEE Trans. Ind. Electron.,* vol. 58, no. 9, pp. 4232 – 4240, Sep. 2011.

[6] M. Makdessi, A. Sari, G. Aubard, P. Venet, C. Joubert, J. Duwattez, "Online health monitoring of metallized polymer film capacitors for avionics applications," *Industrial Electronics (ISIE),* June. 2015, pp.1296-1301.

[7] R. German, A. Sari, P. Venet, M. Ayadi, O. Briat, and J. M. Vinassa, "Prediction of supercapacitors floating ageing with surface electrode interface based ageing law, "*Microelectron. Reliab.*, Aug. 2014.

[8] A. Hammar, P. Venet, R. Lallemand, G. Coquery, G. Rojat, "Study of Accelerated Aging of Supercapacitors for Transport Applications," *IEEE Trans. Ind. Electron.,* vol.57, no.12, pp.3972-3979, Dec. 2010.

[9] E. Schaltz, A. Khaligh, P.O. Rasmussen, "Influence of Battery/Ultracapacitor Energy-Storage Sizing on Battery Lifetime in a Fuel Cell Hybrid Electric Vehicle," *IEEE Trans. Vehicular Technology.,* vol.58, no.8, pp.3882-3891, Oct. 2009

[10] M.W. Ahmad, A. Arya, S. Anand, "An online technique for condition monitoring of capacitor in PV system," *IEEE International Conference on Industrial Technology (ICIT),* March. 2015, pp.920-925.

[11] M. Rigamonti, P. Baraldi, E. Zio, D. Astigarraga, A. Galarza, "Particle Filter-Based Prognostics for an Electrolytic Capacitor Working in Variable Operating Conditions," *IEEE Trans. Ind. Electron.,* vol.31, no.2, pp.1567-1575, Feb. 2016.

[12] P. Kreczanik, P. Venet, A. Hijazi, and G. Clerc, "Study of Supercapacitor Aging and Lifetime Estimation According to Voltage, Temperature, and RMS Current, " *IEEE Trans. Ind. Electron.,*vol. 61, no. 9, pp. 4895–4902, Sep. 2014.

[13] P. Xing-Si, H.N. Thanh, L. Dong-Choon, L. Kyo-Beum, K. Jang-Mok, "Fault Diagnosis of DC-Link Capacitors in Three-Phase AC/DC PWM Converters by Online Estimation of Equivalent Series Resistance," *IEEE Trans. Ind. Electron.,* vol.60, no.9, pp.4118-4127, Sept. 2013.

[14] A.M.R. Amaral and A.J.M. Cardoso, "A Simple Offline Technique for Evaluating the Condition of Aluminum–Electrolytic–Capacitors," *IEEE Trans. Ind. Electron.* vol.56, no.8, pp.3230-3237, Aug. 2009.
[15] M.T. Lawder, B. Suthar, P.W.C. Northrop, S. De, C.M. Hoff, O. Leitermann, M.L. Crow, S. Santhanagopalan, V.R. Subramanian, "Battery Energy Storage System (BESS) and Battery Management System (BMS) for Grid-Scale Applications," *Proceedings of the IEEE* , vol.102, no.6, June 2014. pp.1014-1030.
[16] Z. Shi, F. Auger, E. Schaeffer, P. Guillemet, L. Loron, "Interconnected Observers for online supercapacitor ageing monitoring," *Industrial Electronics Society, IECON 2013*, Nov. 2013, pp.6746-6751.
[17] R. German, A. Hammar, R. Lallemand, A. Sari, P. Venet, "Novel Experimental Identification Method for a Supercapacitor Multipore Model in Order to Monitor the State of Health," *IEEE Trans. Power Electronics.*, vol.31, no.1, pp.548-559, Jan. 2016.
[18] V. Venkat, R. Raghunathan, N. K. Surya , and Y. Kewen,"A review of process fault detection and diagnosis: Part iii: Process history based methods," *Computers & Chemical Engineering.,* vol.27, no.3, pp.327-346, March. 2003.
[19] P.K. Sahoo, R. Panda, P.K. Satpathy, S. Paul, "Voltage stability monitoring based on Feed Forward and Layer Recurrent Neural Networks," *IEEE Power India International Conference (PIICON),* Dec. 2014. pp.1-4.
[20] T. Yamakawa, E. Uchino, T. Miki, H. Kusanagi, "A neo fuzzy neuron and its applications to system identification and prediction of the system behavior," *International conference on Fuzzy Logic and Neural Network, 1992,* pp. 477–483.
[21] T. Kovaltchouk, B. Multon, H. Ben Ahmed, J. Aubry, and P. Venet, "Enhanced Aging Model for Supercapacitors Taking Into Account Power Cycling: Application to the Sizing of an Energy Storage System in a Direct Wave Energy Converter," *IEEE Trans. Ind. Appl.*, vol. 51, no. 3, pp. 2405–2414, May 2015.
[22] H. el Brouji, "Ageing quantification of ultracapacitors during calendar life and power cycling tests using a physically-based impedance model," *IEEE Energy Conversion Congress and Exposition,* 2009, pp. 1791-1798.
[23] H. E. Brouji, O. Briat, J. M. Vinassa, N. Bertrand, and E. Woirgard, "Impact of calendar life and cycling ageing on supercapacitor performance," *IEEE Trans. Veh. Technol.*, vol. 58, pp. 3917–3929, 2009.
[24] H.-K. Song, H.-Y. Hwang, K.-H. Lee, and L. H. Dao, "The effect of pore size distribution on the frequency dispersion of porous electrodes," *Electrochimica Acta*, vol. 45, no. 14, pp. 2241 – 2257, 2000.
[25] O. Bohlen, "Ageing behaviour of electrochemical double layer capacitors Part I. Experimental study and ageing model," *J. Power Sources*, 2007.
[26] M. H. El-husseini, P. Venet, G. Rojat, A. Al-Majid, and M. Fathallah, "Improving pulse handling capability of metalized polypropylene films capacitors," *IEEE Industry Applications Conference,* 2001, vol. 4, pp. 2481–2486.
[27] C. Brinkmann, "Corrosion phenomena on evaporated metal layers under electric stress," *Journal of Materials Science*, vol. 21, pp. 1615-1624, 1986.
[28] R. W. Brown, "Electrical and Thermal Modelling of Low Power Metallised Polypropylene Capacitors," Thesis, RMIT University, 2007.